Research in Astronomy and Astrophysics, 23:085019 (7pp), 2023 August https://doi.org/10.1088/1674-4527/acdabd

Potential for Constraining Propagation Parameters of Galactic Cosmic Rays with the High Energy Cosmic-radiation Detection Facility on Board China's Space Station

Zhi-Hui Xu[1,2], Qiang Yuan[1,2], Zhi-Cheng Tang[3], and Xiao-Jun Bi[3,4]
[1] Key Laboratory of Dark Matter and Space Astronomy, Purple Mountain Observatory, Chinese Academy of Sciences, Nanjing 210023, China; yuanq@pmo.ac.cn
[2] School of Astronomy and Space Science, University of Science and Technology of China, Hefei 230026, China
[3] Key Laboratory of Particle Astrophysics, Institute of High Energy Physics, Chinese Academy of Sciences, Beijing 100049, China
[4] University of Chinese Academy of Sciences, Beijing 100049, China
Received 2023 April 18; revised 2023 May 20; accepted 2023 May 30; published 2023 July 11

Abstract

Precise measurements of the spectra of secondary and primary cosmic rays are crucial for understanding the origin and propagation of those energetic particles. The High Energy Cosmic-radiation Detection (HERD) facility on board China's Space Station, which is expected to operate in 2027, will push the direct and precise measurements of cosmic-ray fluxes up to PeV energies. In this work, we investigate the potential of HERD for studying the propagation of cosmic rays using measurements of boron, carbon, and oxygen spectra. We find that, compared with the current results, the new HERD measurements can improve the accuracy of the propagation parameters by 8%–40%. The constraints on the injection spectra at high energies will also be improved.

Key words: (ISM:) cosmic rays – instrumentation: detectors – The Galaxy

1. Introduction

The origin, acceleration, and propagation of cosmic rays (CRs) remain unresolved despite many years of studies. One of the most important approaches to solving this problem is to measure the energy spectra of various compositions of CRs precisely. Recent precise measurements by mainly direct detection experiments reveal interesting features of many nuclear species, including hardenings around a rigidity of a few hundred GV (Panov et al. 2009; Adriani et al. 2011, 2019, 2020; Aguilar et al. 2015a, 2015b, 2017, 2020; Yoon et al. 2017; An et al. 2019; Alemanno et al. 2021) and softenings around $O(10)$ TV (Atkin et al. 2017; Yoon et al. 2017; An et al. 2019; Alemanno et al. 2021; Albert et al. 2022). For secondary nuclei, which are particularly important in understanding the propagation of CRs, hardening features at similar energies with primary nuclei are also found (Aguilar et al. 2018, 2021; Adriani et al. 2022; Alemanno et al. 2022). This progress in measurements triggered many theoretical studies to discuss new implications for the origin and propagation of CRs (e.g., Ohira & Ioka 2011; Yuan et al. 2011, 2020, 2021; Blasi et al. 2012; Malkov et al. 2012; Tomassetti 2012, 2015; Vladimirov et al. 2012; Thoudam & Hörandel 2014; Cowsik & Madziwa-Nussinov 2016; Guo et al. 2016; Guo & Yuan 2018; Yue et al. 2020; Kawanaka & Lee 2021; Malkov & Moskalenko 2021, 2022; Niu 2022; Ma et al. 2023; Zhang et al. 2023).

The above-mentioned structures are found mainly at relatively low energies. At higher energies (e.g., $\gtrsim$10 TeV), our knowledge about precise spectral structures is still limited. To better understand the propagation properties of CRs, improved measurements in a wider energy range are crucial. The High Energy Cosmic-radiation Detection (HERD) facility, planned to be installed in China's Space Station around 2027, is dedicated to measuring energy spectra of various CR species up to PeV energies (Zhang et al. 2014). The core of the HERD detector is a three-dimensional, five-side active calorimeter (CALO) detector, surrounded by fiber trackers (FITs) for track measurements, plastic scintillator detectors covering the trackers for charge measurements and anticoincidence of γ rays, and silicon charge detectors enclosing all the above subdetectors for charge measurements (Kyratzis & HERD Collaboration 2023). A transition radiation detector is employed to provide energy calibration of nuclei. The geometric factor of HERD is about 2–3 m^2 sr for charged CR detection, and can thus extend the measurements of the spectra of major CR components to >PeV energies. The novel design of HERD makes it a powerful detector for measurements of CR nuclei and electrons/positrons, as well as γ rays in a wide energy range. HERD is expected to significantly advance our understanding of the fundamental problems in CR physics (e.g., to reveal the nature of the knee), as well as to probe new physics such as the nature of dark matter particles (Huang et al. 2016).

In this work, we study the potential for constraining injection and propagation parameters of HERD, assuming a simple one-zone homogeneous propagation model of CRs. We forecast the spectral measurements of boron, carbon, and oxygen CRs

Table 1
Data Used in the Fitting

	Experiment	Time	Modulation	References
B, C, and O	Voyager	2012/12–2015/06	0	Cummings et al. (2016)
	ACE	2011/05–2018/05	ϕ	Yuan (2019)
	AMS-02	2011/05–2018/05	ϕ	Aguilar et al. (2021)
^{10}Be/^{9}Be	IMP	1974/01–1980/05	0.67 GV	Simpson & Garcia-Munoz (1988)
	Voyager	1977/01–1998/12	0.78 GV	Lukasiak (1999)
	ISEE	1978/08–1979/08	0.74 GV	Wiedenbeck & Greiner (1980)
	Ulysses	1990/10–1997/12	0.73 GV	Connell (1998)
	ACE	1997/08–1999/04	0.61 GV	Yanasak et al. (2001)
	ISOMAX	1998/08–1998/08	0.60 GV	Hams et al. (2004)
	PAMELA	2006/07–2014/09	0.57 GV	Nozzoli & Cernetti (2021)

according to the latest designed performance of HERD (Kyratzis & HERD Collaboration 2023), and employ the numerical propagation model GALPROP (Strong & Moskalenko 1998, version 56) together with the Markov Chain Monte Carlo (MCMC) algorithm `emcee`[5] (Foreman-Mackey et al. 2013) to constrain the model parameters. This paper is organized as follows. We describe the framework and setup of the propagation model in Section 2. In Section 3, we present the results of our analysis, focusing on the comparison with current results based on existing data. Finally, we summarize our results and discuss their implications in Section 4.

2. Propagation Model of Cosmic Rays

The propagation of CRs in the Milky Way, which involves a number of physical processes, can be described by the following equation (Ginzburg & Syrovatskii 1964; Strong et al. 2007):

$$\frac{\partial \psi}{\partial t} = \nabla \cdot (D_{xx}\nabla\psi - \boldsymbol{V_c}\psi) + \frac{\partial}{\partial p}p^2 D_{pp}\frac{\partial}{\partial p}\frac{1}{p^2}\psi - \frac{\partial}{\partial p}\left[\dot{p}\psi - \frac{p}{3}(\nabla\cdot\boldsymbol{V_c}\psi)\right] - \frac{\psi}{\tau_f} - \frac{\psi}{\tau_r} + q(\boldsymbol{r}, p), \quad (1)$$

where ψ is the differential density of CRs per momentum interval, D_{xx} is the spatial diffusion coefficient, D_{pp} is the diffusion coefficient in momentum space, which is employed to describe the stochastic reacceleration of CRs, $\boldsymbol{V_c}$ is the convection velocity, $\dot{p}$ is the momentum loss rate, τ_r is the timescale of radioactive decay, τ_f is the timescale of fragmentation, and $q(\boldsymbol{r}, p)$ is the source function.

We assume that the spatial diffusion coefficient, D_{xx}, is spatially homogeneous and depends on the rigidity of particles

[5] https://pypi.org/project/emcee/

Table 2
Fitting Results and 1σ Uncertainties of the Transport and Solar Modulation Parameters

Parameter	Fit without HERD	Fit with HERD
D_0 (10^{28} cm^2 s^{-1})	$4.42^{+0.59}_{-0.53}$	$4.45^{+0.51}_{-0.45}$
δ	$0.426^{+0.010}_{-0.010}$	$0.427^{+0.006}_{-0.006}$
η	$-0.34^{+0.11}_{-0.12}$	$-0.34^{+0.09}_{-0.09}$
z_h (kpc)	$4.32^{+0.64}_{-0.52}$	$4.35^{+0.62}_{-0.48}$
v_A (km s^{-1})	$25.26^{+1.57}_{-1.61}$	$25.25^{+1.19}_{-1.19}$
ϕ (GV)	$0.59^{+0.01}_{-0.01}$	$0.59^{+0.01}_{-0.01}$

Note. Fittings both without and with the HERD data are carried out for comparison.

$\mathcal{R}$ with the power-law form

$$D_{xx}(\mathcal{R}) = D_0\beta^{\eta}\left(\frac{\mathcal{R}}{\mathcal{R}_0}\right)^{\delta}, \quad (2)$$

where $\beta = v/c$ is the velocity of the particle in units of the speed of light, $\mathcal{R}_0 \equiv 4$ GV is a reference rigidity, η is introduced to tune the velocity dependence at low energies to better fit the data, and δ is the slope of the rigidity dependence, which reflects the property of interstellar turbulence (Berezinskii et al. 1990; Schlickeiser 2002). The convective transport is described by a velocity $\boldsymbol{V_c}$, which is the fluid velocity of gas containing relativistic particles. Fitting to the data shows that a high convection velocity is disfavored for reproducing the observed low-energy secondary-to-primary ratios such as B/C (Strong & Moskalenko 1998; Yuan et al. 2017; Yuan 2019). We therefore ignore convection in this work. The scattering of particles off randomly moving magnetohydrodynamic (MHD) waves results in stochastic acceleration of CRs, which can be described by their diffusion in momentum space with the coefficient (Seo & Ptuskin 1994)

$$D_{pp} = \frac{4p^2 v_A^2}{3\delta(4-\delta^2)(4-\delta)wD_{xx}}, \quad (3)$$

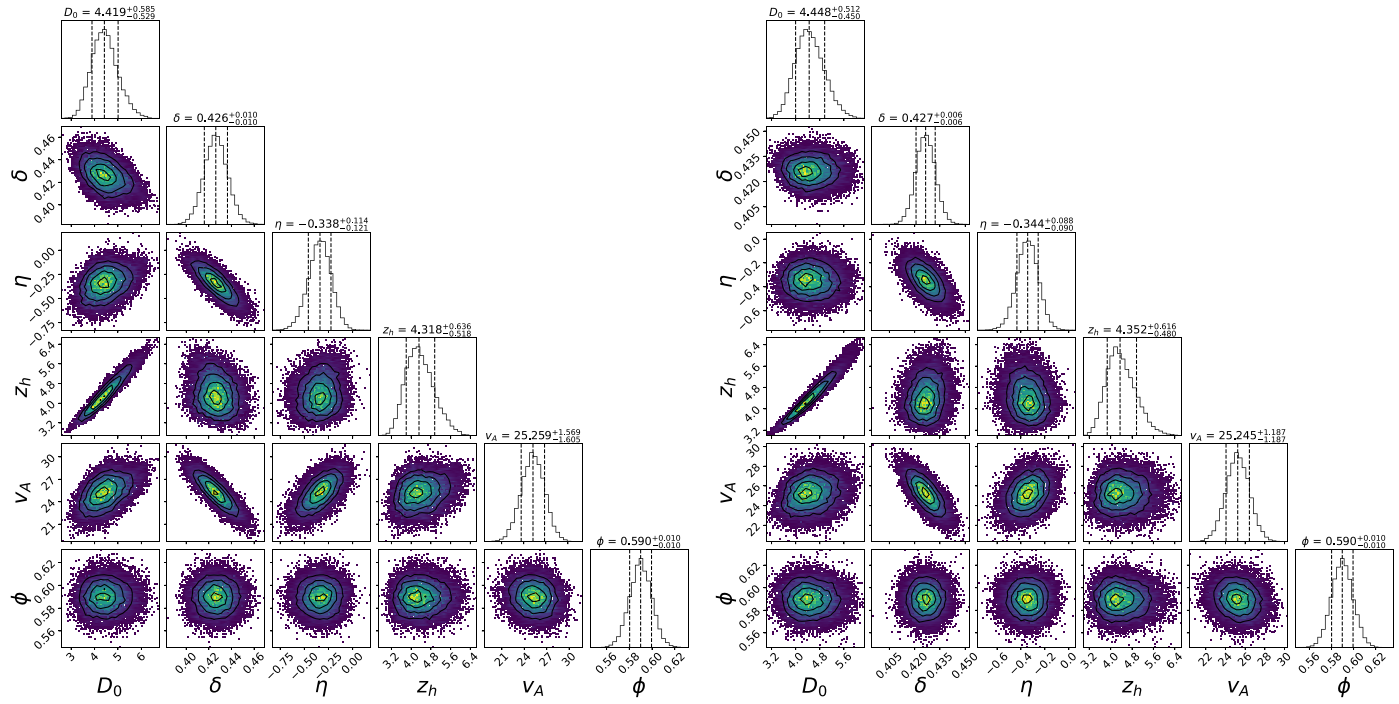

Figure 1. The one-dimensional (diagonal) and two-dimensional (off-diagonal) probability distributions of the propagation parameters. For units of the parameters please refer to Table 2. The left panel is for the fitting to the existing data and the right panel is for the fitting to existing data plus the HERD-predicted spectra.

where v_A is the Alfvén speed of magnetized disturbances; w is the ratio of the energy density of MHD waves to the energy density of the regular magnetic field, and it can be effectively absorbed into v_A.

The spatial distribution of CR sources is assumed to follow the distribution of supernova remnants or pulsars, which is parameterized as the cylindrically symmetric form

$$f(R, z) = \left(\frac{R}{R_\odot}\right)^\alpha \exp\left[-\frac{\beta(R - R_\odot)}{R_\odot}\right] \exp\left(-\frac{|z|}{z_s}\right), \quad (4)$$

where $R_\odot = 8.5$ kpc is the distance from the Earth to the Galactic center, $z_s = 0.2$ kpc is the scale width of the vertical extent of sources, and $\alpha = 1.25$ and $\beta = 3.56$ describe the radial distribution of the sources tuned based on γ rays (Trotta et al. 2011). The source function is truncated at $R_{\rm max} = 20$ kpc and $z_{\rm max} = z_h$, where z_h is the half-height of the propagation halo.

We employ the cubic spline interpolation method in the $\log(\mathcal{R}) - \log(J)$ space to describe the injection spectra of primary CRs (Ghelfi et al. 2016; Zhu et al. 2018). Specifically, we select seven rigidity knots to cover the rigidity range of current measurements:

$$\{\log(\mathcal{R}_1),\ldots,\log(\mathcal{R}_7)\} = \{2.301, 2.968, 3.634, 4.301, 4.968, 5.634, 6.301\}, \quad (5)$$

where the unit of rigidity is MV. Note that the spectral hardening feature at several hundred GV is attributed to the injection spectrum of CRs in this work. Possible breaks in the rigidity dependence of the diffusion coefficient (Vladimirov et al. 2012; Ma et al. 2023) are not considered in the current work. For all primary CRs, the same spectral shape with different abundances is assumed. Finally, the solar modulation, which mainly affects CR spectra at low energies, is applied under the force-field approximation (Gleeson & Axford 1968). The force-field approximation is simplified. Since the solar modulation mainly affects low-energy ($\lesssim$20 GV) spectra of CRs, more complicated modulation models (Potgieter 2013) would have little effect on our conclusion.

3. Analysis and Results

3.1. Fitting to Existing Data

We first run a fitting to existing data, which is used for comparison. The best-fit results of the spectra are also the basis of the prediction of HERD observations. The data used in this work include the spectra of boron, carbon, and oxygen measured by AMS-02 during its first seven years of operation (Aguilar et al. 2021). The low-energy spectra of those species measured by ACE[6] within the same time window

[6] http://www.srl.caltech.edu/ACE/ASC/level2/lvl2DATA_CRIS.html

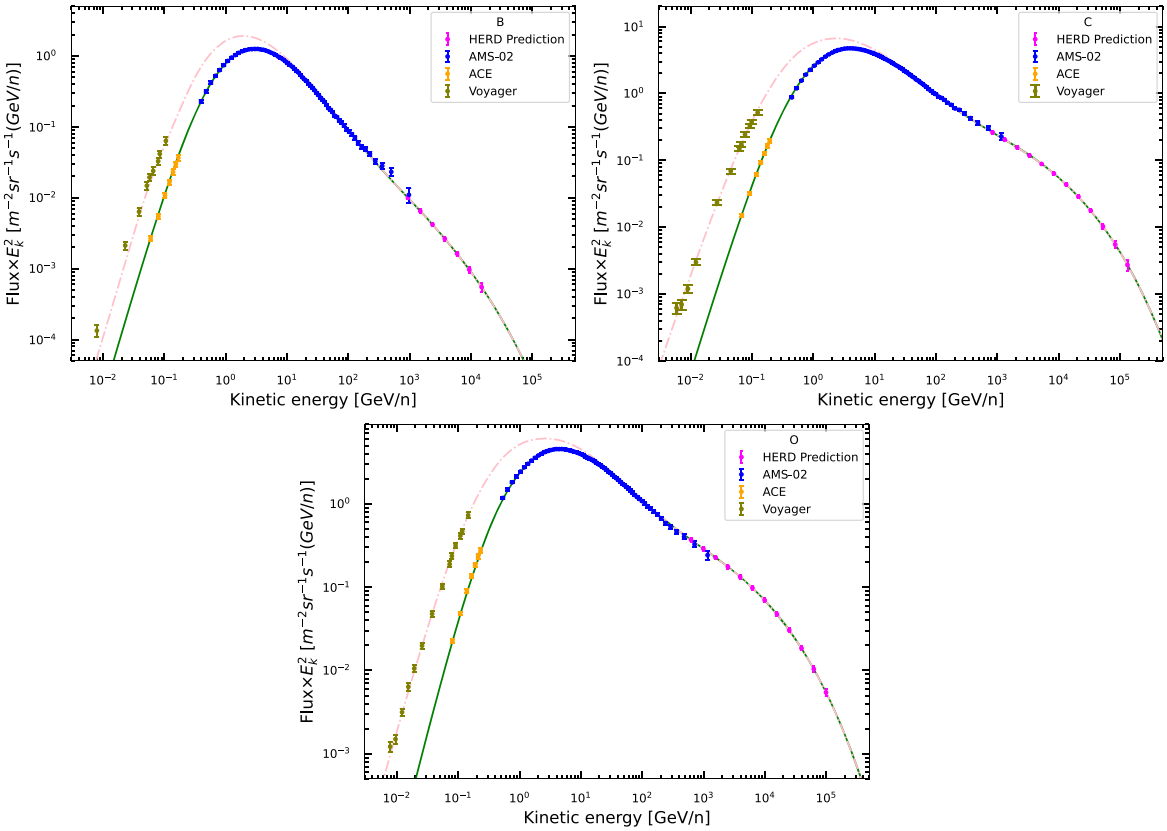

Figure 2. Spectra of boron (top left), carbon (top right), and oxygen (bottom). Lines are the best-fitting results obtained in Section 3.1, with solid (dashed) ones being the spectra after (before) the solar modulation. The HERD-predicted data points are shown by pink dots.

as AMS-02 are extracted (Yuan 2019). Voyager 1 also measured spectra of boron, carbon, and oxygen outside the heliosphere (Cummings et al. 2016), which are helpful in determining the solar modulation parameter. To break the degeneracy between the diffusion coefficient and the halo height, we use the ^{10}Be/^{9}Be ratio measured by several experiments (Wiedenbeck & Greiner 1980; Simpson & Garcia-Munoz 1988; Connell 1998; Lukasiak 1999; Yanasak et al. 2001; Hams et al. 2004; Nozzoli & Cernetti 2021). The observational time periods of ^{10}Be/^{9}Be vary, and thus there are large uncertainties in their solar modulation parameters. We use the modulation potential retrieved from the Cosmic Ray Database[7] (Maurin et al. 2014, 2020), based on the neutron monitor data (Ghelfi et al. 2017). The data are summarized in Table 1.

Our MCMC process involves 14 parameters, consisting of five propagation parameters (D_0, δ, η, z_h, and v_A), six injection spectral parameters, two normalization parameters for carbon and oxygen, and one parameter for solar modulation. The CR nuclei with $Z \leqslant 14$ were included, with normalization parameters being set to the default values of GALPROP except for carbon and oxygen.

The posterior mean and 1σ uncertainties of the propagation parameters and modulation parameter of the fitting are given in Table 2. The one-dimensional distributions and their two-dimensional correlations are shown in the left panel of Figure 1. The best-fitting spectra of boron, carbon, and oxygen, compared with the data, are shown in Figure 2. We note that the derived model parameters are slightly different from those obtained previously, e.g., Yuan et al. (2020). Specifically, the thickness of the propagation halo is smaller, the Alfvén speed is lower, and the parameter δ is bigger in this work than in Yuan et al. (2020). There are several possible reasons for such differences. First, the data of AMS-02 used in this work are the seven-year measurements (Aguilar et al. 2021). Second, we use version 56 of GALPROP in this work, which includes an update of the gas model and results in slightly different production spectra of secondary particles. Third, different data sets used in these works may also result in different constraints on the model parameters. Our results are closer to those given in a recent work (Zhao et al. 2023), where some of the above-mentioned updates have been included.

[7] https://lpsc.in2p3.fr/crdb

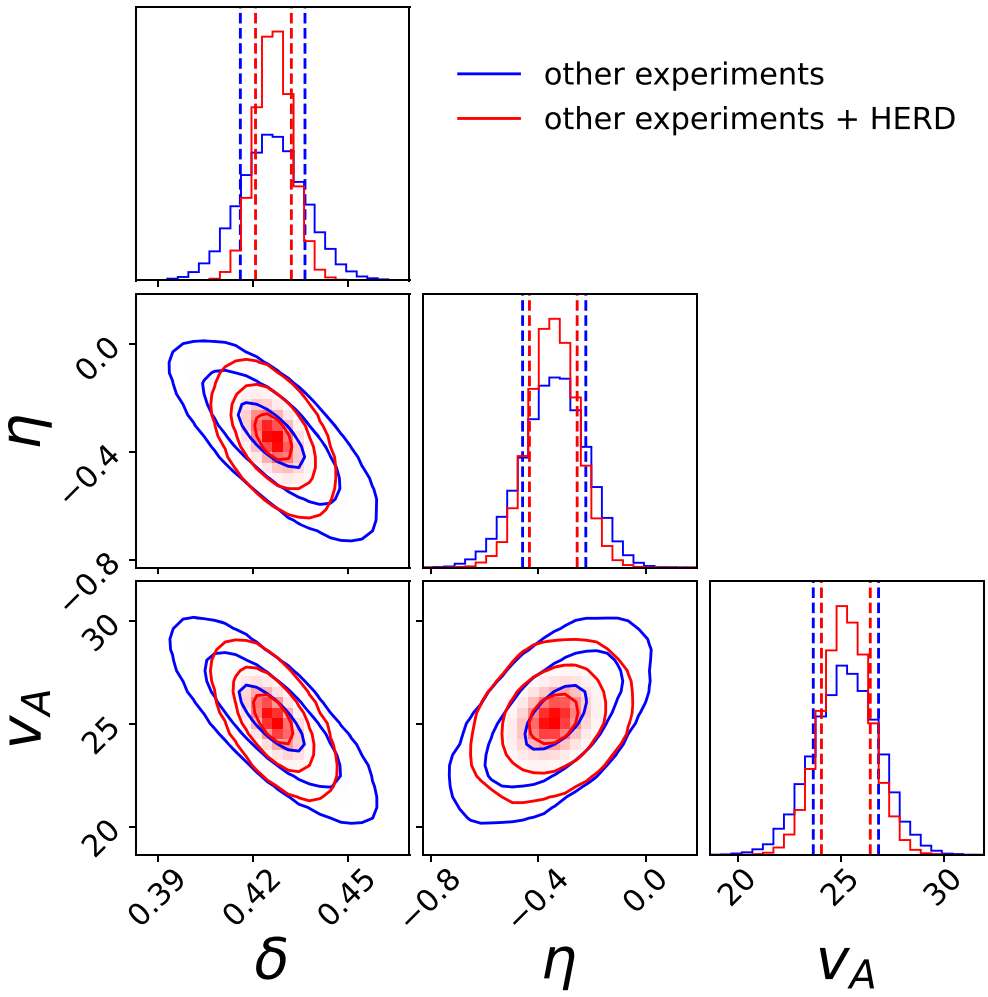

Figure 3. Comparison of the constraints on selected propagation parameters for the fitting without (blue) and with (red) HERD data.

3.2. Predicted Boron, Carbon, and Oxygen Spectra from HERD

Based on the best-fitting spectra of boron, carbon, and oxygen CRs, we predict the HERD measurements. We choose a bin width of $\Delta \log E = 0.2$ for energy, and calculate the expected number of counts in each energy bin based on the simulated effective acceptance of the latest HERD design, for an operational time of 10 years. The effective acceptance takes into account both the geometric factor and the shower development in the CALO based on Monte Carlo simulations. Only the events with early developing showers with sufficient path lengths in the CALO are selected to ensure a good reconstruction quality. To enable a good flux measurement, we further require that the number of events in each energy bin is bigger than 10. Statistical uncertainties and the estimated systematic uncertainties of ∼10% (An et al. 2019; Alemanno et al. 2021) are added in quadrature. We start the HERD spectra from ∼8 TeV, since the spectrometer experiments such as AMS-02 have already measured the spectra with good precision at lower energies. The inclusion of low-energy data points, as long as they are consistent with those of AMS-02, is expected not to change our conclusion significantly. The predicted fluxes measured by HERD, together with other experimental data, are shown in Figure 2.

3.3. Constraints on Model Parameters by Including HERD

We redo the fitting in Section 3.1 to derive the constraints on the model parameters after including the HERD spectra on boron, carbon, and oxygen. The results are given in Table 2 and Figure 1. We find that adding the HERD data will reduce the errors of model parameters by about 8% to 40%. The improvement on the constraint of δ is the most significant. This is expected since HERD mainly improves the measurements at high energies. Note that new measurements of AMS-02 and DAMPE showed hardenings of the B/C and B/O ratios

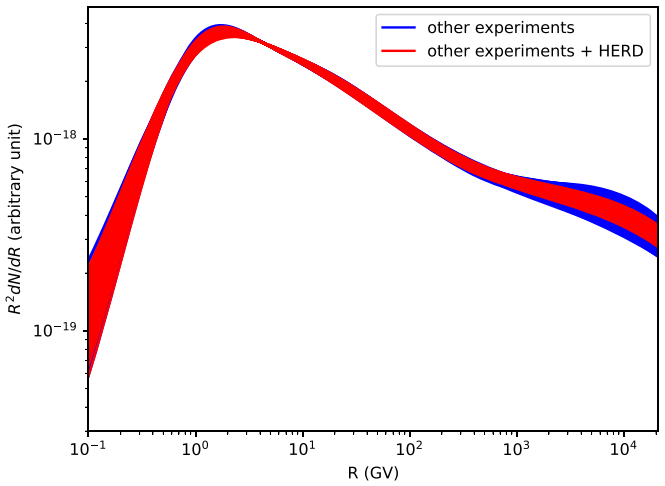

Figure 4. The 1σ bands of injection spectra for the fitting without (blue) and with (red) HERD data.

at high energies (Aguilar et al. 2021; Alemanno et al. 2022), which are not included in this work. However, it is expected that HERD can definitely give better measurements of such ratios above 1 TeV/nucleon, and can thus better constrain the energy dependence of the diffusion coefficient at high energies. There are slight improvements to other propagation parameters, which are mainly determined by low-energy data. Figure 3 compares the constraints on parameters δ, η, and v_A, for the fittings without (blue) and with (red) HERD data.

The inclusion of HERD data at high energies is expected to improve the constraints on the wide-band injection spectra of CRs. Figure 4 shows the comparison of the injection spectra of the two fittings. The shaded bands represent the 1σ spans of the fitting results. As can be seen, the uncertainties above 1 TV are smaller when adding the HERD data.

4. Summary and Discussion

Precise measurements of spectra of primary and secondary CRs in a wide energy range are very important in probing the propagation of Galactic CRs. In this work we study the prospect of constraining CR propagation parameters with the planned HERD mission on board China's Space Station. HERD is expected to measure precisely energy spectra of carbon and oxygen nuclei up to 100 TeV/nucleon and boron nuclei to >10 TeV/nucleon. These measurements are expected to be very helpful in understanding the energy dependence of the diffusion coefficient as well as the injection spectra above 1 TeV/nucleon, which are rarely constrained by existing data.

Under a framework of a continuous source distribution and spatially homogeneous propagation with reacceleration, we fit the boron, carbon, and oxygen data to obtain the constraints on the model parameters. We focus on a comparison of the results for the fittings without and with the HERD data. It is shown that adding the HERD data improves the constraint on the slope parameter (δ) of the energy dependence of the diffusion coefficient significantly. Quantitatively, the error on δ decreases by about 40% after adding the HERD data. Slight improvements to other propagation parameters are also found. In addition, the HERD data are useful in improving the constraints on the injection spectra of primary CRs at high energies.

The model assumption of the current work is simplified. Possible improvements of future works may include (1) study of more secondary (such as lithium, beryllium, fluorine, sub-iron) and primary (oxygen, neon, magnesium, silicon, iron) CR spectra by HERD and particularly the effects of different mass groups (Wu & Chen 2019; Ferronato Bueno et al. 2022; Wang et al. 2022; Zhao et al. 2023), (2) discussion of spectral breaks in the diffusion coefficient (Vladimirov et al. 2012; Ma et al. 2023), and (3) investigation of spatially inhomogeneous propagation as indicated by recent observations (Tomassetti 2012; Guo & Yuan 2018; Zhao et al. 2021).

Acknowledgments

We thank Wei Jiang, Zhao-Qiang Shen, and Cheng-Rui Zhu for the helpful discussion. This work is supported by the National Key Research and Development Program of China (No. 2021YFA0718404), the National Natural Science Foundation of China (No. 12220101003), and the Project for Young Scientists in Basic Research of Chinese Academy of Sciences (No. YSBR-061).

References

Adriani, O., Akaike, Y., Asano, K., et al. 2019, PhRvL, 122, 181102
Adriani, O., Akaike, Y., Asano, K., et al. 2020, PhRvL, 125, 251102
Adriani, O., Akaike, Y., Asano, K., et al. 2022, PhRvL, 129, 251103
Adriani, O., Barbarino, G. C., Bazilevskaya, G. A., et al. 2011, Science, 332, 69
Aguilar, M., Aisa, D., Alpat, B., et al. 2015a, PhRvL, 115, 211101
Aguilar, M., Aisa, D., Alpat, B., et al. 2015b, PhRvL, 114, 171103
Aguilar, M., Ali Cavasonza, L., Alpat, B., et al. 2017, PhRvL, 119, 251101
Aguilar, M., Ali Cavasonza, L., Alpat, B., et al. 2018, PhRvL, 120, 021101
Aguilar, M., Ali Cavasonza, L., Ambrosi, G., et al. 2020, PhRvL, 124, 211102
Aguilar, M., Ali Cavasonza, L., Ambrosi, G., et al. 2021, PhR, 894, 1
Albert, A., Alfaro, R., Alvarez, C., et al. 2022, PhRvD, 105, 063021
Alemanno, F., An, Q., Azzarello, P., et al. 2021, PhRvL, 126, 201102
Alemanno, F., An, Q., Azzarello, P., et al. 2022, SciBu, 67, 2162
An, Q., Asfandiyarov, R., Azzarello, P., et al. 2019, SciA, 5, eaax3793
Atkin, E., Bulatov, V., Dorokhov, V., et al. 2017, JCAP, 7, 020
Berezinskii, V. S., Bulanov, S. V., Dogiel, V. A., & Ptuskin, V. S. 1990, in Astrophysics of Cosmic Rays, ed. V. L. Ginzburg (Amsterdam: Elsevier)
Blasi, P., Amato, E., & Serpico, P. D. 2012, PhRvL, 109, 061101
Connell, J. J. 1998, ApJL, 501, L59
Cowsik, R., & Madziwa-Nussinov, T. 2016, ApJ, 827, 119
Cummings, A. C., Stone, E. C., Heikkila, B. C., et al. 2016, ApJ, 831, 18
Ferronato Bueno, E., Derome, L., Génolini, Y., et al. 2022, arXiv:2208.01337
Foreman-Mackey, D., Hogg, D. W., Lang, D., & Goodman, J. 2013, PASP, 125, 306
Ghelfi, A., Barao, F., Derome, L., & Maurin, D. 2016, A&A, 591, A94
Ghelfi, A., Maurin, D., Cheminet, A., et al. 2017, AdSpR, 60, 833
Ginzburg, V. L., & Syrovatskii, S. I. 1964, The Origin of Cosmic Rays (New York: Macmillan)
Gleeson, L. J., & Axford, W. I. 1968, ApJ, 154, 1011
Guo, Y.-Q., Tian, Z., & Jin, C. 2016, ApJ, 819, 54

Guo, Y.-Q., & Yuan, Q. 2018, PhRvD, 97, 063008
Hams, T., Barbier, L. M., Bremerich, M., et al. 2004, ApJ, 611, 892
Huang, X., Lamperstorfer, A. S., Tsai, Y.-L. S., et al. 2016, APh, 78, 35
Kawanaka, N., & Lee, S.-H. 2021, ApJ, 917, 61
Kyratzis, D. & HERD Collaboration 2023, NIMPA, 1048, 167970
Lukasiak, A. 1999, ICRC, 3, 41
Ma, P.-X., Xu, Z.-H., Yuan, Q., et al. 2023, FrPhy, 18, 44301
Malkov, M. A., Diamond, P. H., & Sagdeev, R. Z. 2012, PhRvL, 108, 081104
Malkov, M. A., & Moskalenko, I. V. 2021, ApJ, 911, 151
Malkov, M. A., & Moskalenko, I. V. 2022, ApJ, 933, 78
Maurin, D., Dembinski, H. P., Gonzalez, J., Mariś, I. C., & Melot, F. 2020, Universe, 6, 102
Maurin, D., Melot, F., & Taillet, R. 2014, A&A, 569, A32
Niu, J.-S. 2022, ApJ, 932, 37
Nozzoli, F., & Cernetti, C. 2021, Universe, 7, 183
Ohira, Y., & Ioka, K. 2011, ApJL, 729, L13
Panov, A. D., Adams, J. H., Ahn, H. S., et al. 2009, BRASP, 73 564
Potgieter, M. S. 2013, LRSP, 10, 3
Schlickeiser, R. 2002, Cosmic Ray Astrophysics (Berlin: Springer)
Seo, E. S., & Ptuskin, V. S. 1994, ApJ, 431, 705
Simpson, J. A., & Garcia-Munoz, M. 1988, SSRv, 46, 205
Strong, A. W., & Moskalenko, I. V. 1998, ApJ, 509, 212
Strong, A. W., Moskalenko, I. V., & Ptuskin, V. S. 2007, ARNPS, 57, 285
Thoudam, S., & Hörandel, J. R. 2014, A&A, 567, A33
Tomassetti, N. 2012, ApJL, 752, L13
Tomassetti, N. 2015, ApJL, 815, L1
Trotta, R., Jóhannesson, G., Moskalenko, I. V., et al. 2011, ApJ, 729, 106
Vladimirov, A. E., Jóhannesson, G., Moskalenko, I. V., & Porter, T. A. 2012, ApJ, 752, 68
Wang, Y., Wu, J., & Long, W.-C. 2022, ChPhC, 46, 095102
Wiedenbeck, M. E., & Greiner, D. E. 1980, ApJL, 239, L139
Wu, J., & Chen, H. 2019, PhLB, 789, 292
Yanasak, N. E., Wiedenbeck, M. E., Mewaldt, R. A., et al. 2001, ApJ, 563 768
Yoon, Y. S., Anderson, T., Barrau, A., et al. 2017, ApJ, 839, 5
Yuan, Q. 2019, SCPMA, 62, 49511
Yuan, Q., Lin, S.-J., Fang, K., & Bi, X.-J. 2017, PhRvD, 95, 083007
Yuan, Q., Qiao, B.-Q., Guo, Y.-Q., Fan, Y.-Z., & Bi, X.-J. 2021, FrPhy, 16, 24501
Yuan, Q., Zhang, B., & Bi, X.-J. 2011, PhRvD, 84, 043002
Yuan, Q., Zhu, C.-R., Bi, X.-J., & Wei, D.-M. 2020, JCAP, 2020, 027
Yue, C., Ma, P.-X., Yuan, Q., et al. 2020, FrPhy, 15, 24601
Zhang, P.-P., He, X.-Y., Liu, W., & Guo, Y.-Q. 2023, JCAP, 02, 007
Zhang, S. N., Adriani, O., Albergo, S., et al. 2014, Proc. SPIE, 9144, 91440X
Zhao, M.-J., Bi, X.-J., & Fang, K. 2023, PhRvD, 107, 063020
Zhao, M.-J., Fang, K., & Bi, X.-J. 2021, PhRvD, 104, 123001
Zhu, C.-R., Yuan, Q., & Wei, D.-M. 2018, ApJ, 863, 119